

1 **Author comments**

2  
3 Atmos. Meas. Tech. Discuss., 7, 171–194, 2014

4 **DIAL measurement of lower tropospheric ozone over Saga (33.24°N, 130.29°E), Japan,**  
5 **and comparison with a chemical climate model,**

6 by O. Uchino, T. Sakai, T. Nagai, I. Morino, T. Maki, M. Deushi, K. Shibata, M. Kajino,  
7 T. Kawasaki, T. Akaho, S. Takubo, H. Okumura, K. Arai, M. Nakazato, T. Matsunaga, T.  
8 Yokota, S. Kawakami, K. Kita, and Y. Sasano

9  
10 The authors wish to thank two referees and Prof. M. J. Newchurch for helpful and  
11 thoughtful comments. Each comment is addressed individually below. The referee  
12 comments are written in black, and our responses are described in red.

13 The main changes of the paper since the APCD version are:

- 14 ● We add a new figure after Fig.5.

15 **Fig. 6.** Horizontal maps of ozone volume mixing ratio in ppbv and horizontal wind in  
16 m/s predicted by MRI-CCM2 for 500, 700, 800, 850 hPa pressure levels at 06 h UTC  
17 on 7 July 2012.

18 Therefore, figure number for Fig. 6 is changed to Fig.7.

19  
20 **Review of manuscript by Anonymous Referee #2**

21 **General Remarks**

22 The manuscript describes an upgraded version of an existing ozone lidar system. The  
23 performance of the system seems to be good. The value of lidar vertical sounding for  
24 model validation and synergetic use is demonstrated. However, some more literature on  
25 the benefit of model validation with lidar systems should be included. If a longer effort  
26 is planned this should be mentioned since in the past just single case studies have been  
27 made. I recommend publication after a few minor adjustments.

28  
29 We included next three papers in References and our plan after line 19 in Sec. 5 in P.  
30 183:

31  
32 Roelofs, G. J., Kentarchos, A. S., Trickl, T., Stohl, A., Collins, W. J., Crowther, R. A.,  
33 Hauglustaine, D., Klonecki, A., Law, K. S., Lawrence, M. G., von Kuhlmann, R., and  
34 van Weele, M.: Intercomparison of tropospheric ozone models: ozone transport in a  
35 complex tropopause folding event, *J. Geophys. Res.*, 108, D12, 8529,  
36 doi:10.1029/2003JD003462, 2003.

- 1 Zanis, P., Trickl, T., Stohl, A., Wernli, H., Cooper, O., Zerefos, C., Gaeggeler, H., Schnabel,  
2 C., Tobler, L., Kubik, P. K., Priller, A., Scheel, H. E., Kanter, H. J., Cristofanelli, P.,  
3 Forster, C., James, P., Gerasopoulos, E., Delcloo, A., Papayannis, A., and Claude, H.:  
4 Forecast, observation and modeling of a deep stratospheric intrusion event over  
5 Europe, *Atmos. Chem. Phys.*, 3, 763-777, 2003.
- 6 Niwano, M., Takigawa, M., Takahashi, M., Akimoto, H., Nakazato, M., Nagai, T., Sakai,  
7 T., and Mano, Y.: Evaluation of vertical ozone profiles simulated by WRF/Chem using  
8 lidar-observed data, *SOLA*, 3, 133-136, doi:10.2151/sola.2007-034, 2007.

9  
10  
11 A major benefit of ozone DIAL is that it can measure continuously vertical ozone  
12 profiles with high vertical and temporal resolution. The process of stratospheric ozone  
13 intrusion into the troposphere was clearly observed on 20-21 June 2001 by continuous  
14 DIAL measurement at Garmisch-partenkichen, Germany and the excellent data set  
15 was used for model intercomparisons and validation (Roelofs et al., 2003; Zanis et al.,  
16 2003; Stohl et al., 2003). On the other hand, the ability of a regional air quality model  
17 was evaluated to reproduce summertime ozone pollution over the Kanto region in Japan  
18 using quasi-continuous ozone DIAL measurement data (Niwano et al, 2007). We plan to  
19 study the process that air mass of high ozone concentration in the free troposphere is  
20 mixed into the planetary boundary layer by continuous DIAL measurement. Further,  
21 we plan to utilize ozone DIAL data for validation of a new version of an MRI oxidant  
22 prediction system over an extended period of time. In the prediction system, a regional  
23 chemistry-transport model, known as MRI-PM/c (Kajino et al., 2012), with higher  
24 spatial resolution (20 km and/or 5 km) is nested in MRI-CCM2. The prediction system  
25 also adopts an up-to-date inventory and higher temporal resolution of biomass burning  
26 emissions. The regional model can reproduce meso-scale weather phenomena and  
27 advection of air mass. However, if boundary data for the regional model produced by the  
28 global model doesn't include adequate information on fine-scale structures in trace gas  
29 distributions, the performance of the prediction system will be degraded. Therefore, in  
30 order to improve total performance of the prediction system, it is necessary to validate  
31 not only the regional model but also the global model with observation data such as  
32 ozone DIAL data and surface ozone monitoring data extensively, which enable us to  
33 estimate error coming from outside of the boundary.

## 34 35 36 **Details**

1 (1) P. 173, line 22: Replace "pollution" by "pollutant".  
2 **Done**

3 (2) P. 175 line 21: I suggest writing: "we modified the coaxial receiving system by adding  
4 a small telescope in biaxial configuration".  
5 **We changed to "we modified the coaxial receiving system by adding a mirror in biaxial  
6 configuration"**

7 (3) P. 178, lines 3-4: Please, replace "systematic error" by "systematic uncertainty". A  
8 systematic error is a known quantity and must be corrected!  
9 **Done**

10 (4) P. 181, lines 21-22: "A regional model....might solve these discrepancies": Such a  
11 statement requires more information on the air masses. For instance, it could be the  
12 case that air from different sources arrives side by side. This can be clarified by  
13 trajectory analyses or by looking at the model output for adjacent grid boxes. A  
14 smaller-scale model is helpful, if air filaments from outside the model domain of the  
15 fine-scale model are captured to some extent by the larger-scale model. Otherwise they  
16 are missed! I suggest improving also the corresponding part of the "Concluding  
17 remarks".  
18

19 **Instead of the sentence "A regional model with a higher spatial resolution of 20 km  
20 might solve these discrepancies" in P.181, line 21, we added following sentences with  
21 Fig.6:**  
22

23 **Figure 6 shows horizontal maps of ozone volume mixing ratio and horizontal wind  
24 predicted by MRI-CCM2 for 500 hPa (about 5.5 km altitude), 700 hPa (3 km), 800 hPa (2  
25 km), and 850 hPa (1.5 km) pressure levels at 06 UTC on 7 July 2012. According to the  
26 weather chart on the same day provided by JMA  
27 (<http://www.data.jma.go.jp/fcd/yoho/hibiten/index.html>), the Meiyu-Baiu-front extended  
28 from west to east through the center of a low-pressure system over Japan. In this  
29 prediction, the synoptic-scale pattern of horizontal-wind field is reproduced reasonably.  
30 A large north-south gradient of ozone volume mixing ratios is located near the  
31 stationary front in the lower free-troposphere. The ozone concentration is low over the  
32 south part of the front because of the chemical destruction in the summertime marine  
33 air mass, whereas high ozone level area is present over the north of the front. During  
34 the DIAL observing period the large gradient of ozone concentration was located near  
35 the Saga site in the lower free-troposphere (Fig.6). This suggests that one of the possible  
36 reasons for the significant discrepancy between the DIAL ozone profile and the**

1 predicted one (Fig. 5) is that the meso-scale front structure and its position were not  
2 fully captured by the model due to its coarse spatial resolution. In addition, it is  
3 plausible that model transport with the coarse grid doesn't reproduce well fine-scale  
4 structures of air (trace gases) filaments.

5  
6 (5) P. 182, line 8: Replace "exchanges" by "exchange" (or perhaps "exchange events").

7 We replaced to "exchange events".

8 (6) Sec. 5: There is no clear statement about future plans or work. The use of the  
9 regional model is sold as an option, not as a plan. Given the uncertainties of regional  
10 models with air parcels coming from remote sources mentioned above it is also  
11 advisable to announce further comparisons and optimization (see general remarks).

12 We included future plans in Sec. 5.

13  
14  
15 **Review of manuscript by Anonymous Referee #1**

16 We corrected many sentences in intelligible terms which are recommended by Referee  
17 #1. We understood the main comments by Referee are as follows:

18  
19 1) Add some numerical values in DU in Abstract and Concluding remarks

20 We added some numerical values in DU in Abstract and Concluding remarks.

21 2) Problem in page 176, line 22: 1 single lens is not enough for such a wide spectral  
22 range (chromatic aberration) provide comment please.

23 It might be better to use an off-axis beam expander for a wide spectral range of 276–312  
24 nm. We would like to study this matter further.

25  
26 3) Normally Raman energies are  $S_1 > S_2 > S_3$ , so explain why  $S_1 < S_3$

27 At a pumping energy of 107 mJ at 266 nm,

28  $S_1:S_2:S_3=10.0:10.1: 4.7$  mJ ( $S_1+S_2+S_3=24.8$  mJ) for  $8.1 \times 10^5$  Pa of CO<sub>2</sub> gas (8 atm.),

29 and

30  $S_1:S_2:S_3=7.5:9.1: 8.4$  mJ ( $S_1+S_2+S_3=25.0$  mJ) for  $3.0 \times 10^5$  Pa of CO<sub>2</sub> gas (3 atm.).

31 As the total energies were almost the same (about 25 mJ), our experimental result was  
32 correct. The reason why  $S_1 < S_3$  is beyond the scope of this paper. We would like to study  
33 further the reason.

34 4) Why didn't you make measurement of the output energy at  $S_4:312$  nm?

35 It was difficult for us to measure the output energy at 312 nm in September 2012 due to  
36 the limited space in the container and the maximum output energy of 107 mJ at 266 nm

1 could not be obtained.

2 5) Add references

3 We added next three papers in References:

4  
5 Papayannis, A., Ancellet, G., Pelon, J., and Mégie, G.: Multiwavelength lidar for ozone  
6 measurements in the troposphere and the lower stratosphere, *Appl. Opt.*, 29, 467-476,  
7 1990.

8 Papayannis, A., Balis, D., Zanis, P., Galani, E., Wernli, H., Zerefos, C., Stohl, A.,  
9 Eckhardt, S., and Amiridis, V.: Sampling of an STT event over the Eastern  
10 Mediterranean region by lidar and electrochemical sonde, *Annales Geophys.*, 23,  
11 2039-2050, 2005.

12 Stohl, A., Bonasoni, P., Cristofanelli, P., Collins, W., Feichter, J., Frank, A., Forster, C.,  
13 Gerasopoulos, E., Gäggeler, H., James, P., Kentarchos, T., Kromp-Kolb, H., Krüger,  
14 B., Land, C., Meloan, J., Papayannis, A., Priller, A., Seibert, P., Sprenger, M., Roelofs,  
15 G. J., Scheel, H. E., Schnabel, C., Siegmund, P., Tobler, L., Trickl, T., Wernli, H.,  
16 Wirth, V., Zanis, P., and Zerefos, P.: Stratosphere-troposphere exchange: a review,  
17 and what we have learned from STACCATO, *J. Geophys. Res.*, 108, D12, 8516,  
18 doi:10.1029/2002JD002490, 2003.

19  
20 **Interactive comment on Atmos. Meas. Tech. Discuss.**, 7, 171-194, 2014.

21 **M. J. Newchurch**

22 mike@nsstc.uah.edu

23 Received and published: 30 January 2014

24 We are very pleased to see this Japanese tropospheric ozone lidar obtaining data. As  
25 one of a very small number of tropospheric ozone lidars (e.g., TOLNet:  
26 <http://wwwair.larc.nasa.gov/missions/TOLNet/>) its contribution will have a large impact  
27 on the global available ozone lidar data available for scientific studies.

28 I have two suggestions for the authors to strengthen this paper:

29 1) Provide quantitative estimates of the accuracy of the lidar retrievals relative to the  
30 correlative observations (means, s.d., function of altitude, etc.).

31 We added following sentence after Page.178, line 21:

32 The average and one standard deviation of the difference between DIAL and ozonesonde  
33 data are 14±10 % below 2 km, 6±4 % for 2–7 km, and 20±13 % above 7 km.

34  
35 2) Provide some example(s) of time/altitude plots of the temporal progression of  
36 tropospheric ozone over your sight (e.g.,

1 <http://nsstc.uah.edu/atmchem/lidar/data/120606/120606.html>).

2 We would encourage you to continue to strive for data at lower altitudes (e.g.,  $\leq 100\text{m}$   
3 AGL) and during interesting geophysical conditions (diurnal PBL development, STE,  
4 land/ocean interactions, etc.). We look forward to future publications of these lidar  
5 observations.

6  
7 As denoted in Sec. 5, we plan to study the process that air mass of high ozone  
8 concentration in the free troposphere is mixed into the planetary boundary layer by  
9 continuous DIAL measurement. In the process study, we would like to provide some  
10 examples of time/altitude plots of the temporal progression of tropospheric ozone.  
11 We thank you for your encouragement of our ozone DIAL measurement in Japan.

12  
13  
14  
15  
16  
17  
18  
19  
20  
21  
22  
23  
24  
25  
26  
27  
28  
29  
30  
31  
32  
33  
34  
35  
36

1 **Revised manuscript**

2  
3 **DIAL measurement of lower tropospheric ozone over Saga (33.24°N, 130.29°E),**  
4 **Japan, and comparison with a chemistry climate model**

5  
6 O. Uchino<sup>1, 2</sup>, T. Sakai<sup>2</sup>, T. Nagai<sup>2</sup>, I. Morino<sup>1</sup>, T. Maki<sup>2</sup>, M. Deushi<sup>2</sup>, K. Shibata<sup>2</sup>, M.  
7 Kajino<sup>2</sup>, T. Kawasaki<sup>3</sup>, T. Akaho<sup>3</sup>, S. Takubo<sup>3</sup>, H. Okumura<sup>3</sup>, K. Arai<sup>3</sup>, M. Nakazato<sup>4</sup>, T.  
8 Matsunaga<sup>1</sup>, T. Yokota<sup>1</sup>, S. Kawakami<sup>5</sup>, K. Kita<sup>6</sup>, and Y. Sasano<sup>1</sup>

9  
10 <sup>1</sup>National Institute for Environmental Studies, 16-2 Onogawa, Tsukuba, Ibaraki  
11 305-8506

12 <sup>2</sup>Meteorological Research Institute, 1-1 Nagamine, Tsukuba, Ibaraki 305-0052, Japan

13 <sup>3</sup>Saga University, 1 Honjou, Saga, Saga 840-8502, Japan

14 <sup>4</sup>Japan Meteorological Agency, 1-3-4 Otemachi, Chiyoda-ku, Tokyo 100-8122, Japan

15 <sup>5</sup>Japan Aerospace Exploration Agency, 2-1-1 Sengen, Tsukuba, Ibaraki 305-8505, Japan

16 <sup>6</sup>Ibaraki University, 2-1-1 Bunkyo, Mito, Ibaraki 310-8512, Japan

17  
18 Correspondence to: O. Uchino (uchino.osamu@nies.go.jp)

## 1 Abstract

2 We have improved an ozone Differential Absorption Lidar (DIAL) system, originally  
3 developed in March 2010. The improved DIAL system consists of a Nd:YAG laser and a  
4 2 m Raman cell filled with  $8.1 \times 10^5$  Pa of CO<sub>2</sub> gas which generate four Stokes lines (276,  
5 287, 299, and 312 nm) of stimulated Raman scattering, and two receiving telescopes  
6 with diameters of 49 and 10 cm. Using this system, 44 ozone profiles were observed in  
7 the 1–6 km altitude range over Saga (33.24°N, 130.29°E) in 2012. High ozone layers  
8 were observed at around 2 km altitude during April and May. Ozone column amounts  
9 within the 1–6 km altitude range were almost constant (19.1 DU on average) from  
10 January to March, and increased to 26.7 DU from late April to July. From mid-July  
11 through August, ozone column amounts decreased greatly to 14.3 DU because of  
12 exchanges of continental and maritime air masses. Then in mid-September they  
13 increased again to 22.1 DU within 1–6 km, and subsequently decreased slowly to 17.3  
14 DU, becoming almost constant by December.

15 The Meteorological Research Institute's Chemistry-Climate Model version 2  
16 (MRI-CCM2) successfully predicted most of these ozone variations with the following  
17 exceptions. MRI-CCM2 could not predict the high ozone volume mixing ratios measured  
18 at around 2 km altitude on 5 May and 11 May, possibly in part because emissions were  
19 assumed in the model to be constant (climatological data were used). Ozone volume  
20 mixing ratios predicted by MRI-CCM2 were low in the 2–6 km range on 7 July and high  
21 in the 1–4 km range on 19 July compared with those measured by DIAL.

## 25 1 Introduction

27 Ozone is an important air pollutant that at high concentrations impacts on human  
28 health and ecosystems including crops (Parrish et al., 2012). Tropospheric ozone has two  
29 main sources: photochemical production in the troposphere and downward transport  
30 from the stratosphere. Tropospheric ozone is mainly produced from nitrogen oxides  
31 (NO<sub>x</sub>), carbon monoxide (CO), and volatile organic compounds (VOCs) by photochemical  
32 reactions. More specifically in Asia, emissions of these ozone precursors increased  
33 between 1980 and 2003 (Ohara et al., 2007). In China in particular, NO<sub>x</sub> increased from  
34 1996 through 2004 (Zhang et al., 2007). Summertime ozone concentrations in the 0–3  
35 km altitude range over Beijing increased at the rate of 3 % yr<sup>-1</sup> from 2002 to 2010 (Wang  
36 et al., 2012). Ozone is also a greenhouse gas that plays an important role in climate

1 change. The radiative forcing due to tropospheric ozone is the third strongest after  
2 carbon dioxide and methane (IPCC, 2007).

3 In recent years, high concentrations of surface ozone have been observed from April  
4 through June in the Kyushu district of western Japan (<http://www.env.go.jp/air/osen/>).  
5 In 2011, we deployed an ozone Differential Absorption Lidar (ozone DIAL) system,  
6 originally developed by the National Institute for Environmental Studies (NIES) at  
7 Tsukuba, at Saga (33.24°N, 130.29°E) in the Kyushu district, with three aims: (1) to  
8 validate GOSAT (Greenhouse gases Observing SATellite) ozone products retrieved from  
9 thermal infrared spectral radiances by the Thermal And Near infrared Sensor for  
10 carbon Observation-Fourier Transform Spectrometer (TANSO-FTS) onboard GOSAT  
11 (Ohyama et al., 2012); (2) to detect high ozone concentrations in the lower troposphere;  
12 and (3) to compare the observed concentrations with concentration data predicted by  
13 the Meteorological Research Institute's (MRI) Chemistry-Climate Model, version 2  
14 (MRI-CCM2) (Deushi and Shibata, 2011). Except in summer, Saga is downwind of the  
15 Asian continent most of the year. Thus, if DIAL can be used to detect high ozone  
16 concentrations, then inputting DIAL data into MRI-CCM2 will allow us to make useful  
17 predictions for photochemical oxidant advisories. In Sect. 2 we describe the ozone DIAL  
18 system, including some improvements made since 2011 and comparisons with  
19 ozonesonde data, and we describe MRI-CCM2 in Sect. 3. In Sect. 4, we present  
20 observational results obtained by the ozone DIAL system and compare them with  
21 MRI-CCM2 predictions. Section 5 is a summary and our conclusions.

## 22 23 24 **2 Ozone DIAL system, data analysis and comparison with ozonesonde results**

25  
26 Tropospheric ozone DIAL systems have been first developed using tunable dye lasers  
27 (Gibson and Thomas, 1975; Pelon and Mégie, 1982; Browell et al., 1983; Profitt and  
28 Langford, 1997; Kuang et al., 2013). Later Stokes lines from stimulated Raman  
29 scattering (SRS) of pressurized gas pumped by excimer lasers (Uchino et al., 1983;  
30 Kempfer et al., 1994; Eisele et al., 1999), and by Nd:YAG lasers (Ancellet et al., 1989;  
31 Sunesson et al., 1994; McDermid et al., 2002; [Papayannis et al., 2005](#); Nakazato et al.,  
32 2007; Apituley et al., 2010) were used. In 2010, we developed a tropospheric ozone DIAL  
33 system at NIES (Uchino et al., 2011) that was installed in a container with dimensions  
34 of about 228 cm × 683 cm × 255 cm. The system's transmitter transmits laser beams at  
35 three Stokes lines (276.2 nm, 287.2 nm, and 299.1 nm) of the SRS of carbon dioxide  
36 (CO<sub>2</sub>) [with vibrational shift of 1385 cm<sup>-1</sup>](#) pumped by the fourth harmonic (266 nm) of a

1 Nd:YAG laser (Nakazato et al., 2007; Seabrook et al., 2011).

2 We used this transmitter with a coaxial receiving system with a 49 cm-diameter  
3 Newtonian reflecting telescope to measure ozone profiles from a few hundred meters to  
4 about 10 km altitude. However, the signal-induced bias (SIB) from the photomultiplier  
5 tubes (PMTs) limited the measurement altitude to below about 6 km (Sunesson et al.,  
6 1994; Proffitt and Langford, 1997). A mechanical chopper with a fast rising time could  
7 suppress the SIB (Uchino and Tabata, 1991; McDermid et al., 2002; Godin-Beekmann et  
8 al., 2003; Apituley et al., 2010), but there was not enough space in the container to add a  
9 mechanical chopper to the DIAL receiving system. Therefore, in January 2012 we  
10 modified the coaxial receiving system by adding a mirror in biaxial configuration. In the  
11 biaxial system, the Stokes lines were transmitted upward by a 10 cm-diameter mirror  
12 with 90 % reflectivity that was set at a distance of 25 cm from the edge of the 49 cm  
13 telescope, while about 10 % of the laser energy was used to measure low-altitude ozone  
14 by the original coaxial system. Thus adding the biaxial system, we could measure ozone  
15 profiles up to about 10 km; However, it was time-consuming to measure ozone profiles  
16 from 1 to 10 km by alternating between biaxial and coaxial measurements.

17 To be able to measure tropospheric ozone profiles simultaneously in the altitude  
18 range of 0.3–10 km, we introduced an additional new 10 cm-diameter Newtonian  
19 receiving telescope in September 2012, using a 1.8 mm-diameter quartz optical fiber to  
20 transmit the receiving light from the position of the iris of the 10 cm telescope to the  
21 entrance of a spectrometer. A dichroic beamsplitter with a 15° incidence angle efficiently  
22 separated the signal into two wavelengths, 276 and 287 nm. Furthermore, we tested the  
23 use of a fourth Stokes line (312.0 nm) of SRS from CO<sub>2</sub> for ozone measurement up to  
24 15–20 km on a clear night by two wavelengths of 299 and 312 nm.

25 A block diagram of the improved DIAL system is shown in Fig. 1. The maximum  
26 output pulse energy of the Nd:YAG laser (Quantel YG981C) is 107 mJ per pulse at 266  
27 nm; However the normal averages of the output energies are 70–85 mJ at 266 nm. The  
28 laser beam is collimated into the center of a 2 m-long Raman cell, which consists of a  
29 stainless-steel tube with a diameter of 35 mm and 10 mm-thick UV-grade quartz  
30 windows with an anti-reflective (AR) coating. The input window is a lens with a focal  
31 length  $f_1=1100$  mm. The output energy at 312.0 nm is not measured, but CO<sub>2</sub> pressure is  
32 set to be  $8.1 \times 10^5$  Pa because the largest receiving signal is obtained at 312.0 nm. At  $8.1$   
33  $\times 10^5$  Pa of CO<sub>2</sub> pressure and a pumping energy of 107 mJ at 266 nm, the output  
34 energies of the three Stokes lines at S1: 276.2, S2: 287.2, and S3: 299.1 nm are 7.5, 9.1,  
35 and 8.4 mJ, respectively. A pumping energy of more than 90 mJ at 266 nm is necessary  
36 for DIAL measurement using the Stokes lines at 299 nm and 312 nm.

1 The four Stokes lines are expanded by a factor of about 3.9 by a 50 mm-diameter  
2 quartz lens with a focal length  $f_2=4290$  mm. The beam divergence of the four Stokes  
3 lines transmitted into the atmosphere is about 0.1 mrad. The full field of views of the 49  
4 cm and 10 cm telescope are 1.0 and 3.0 mrad, respectively. The system uses PMTs  
5 (Hamamatsu R3235) to detect the backscattered light from the atmosphere. For signal  
6 processing, a 12-bit A/D converter and photon counter (Licel TR20-160) are used. The  
7 timing of the DIAL system is controlled by a delay/pulse generator (Stanford Research  
8 Systems DG645). The specifications of this ozone DIAL system are summarized in Table  
9 1.

10 The ozone number density is derived from the DIAL signals at the two wavelengths  
11 (Uchino and Tabata, 1991). The raw data were obtained with 7.5 m range resolution and  
12 1 min integration time (i.e., 600 shots). The analog and photon counting signals for each  
13 receiving wavelength channel in Fig. 1 were connected to get high dynamic range. To  
14 increase the signal-to-noise ratio, the integrated spatial range interval ( $\Delta z$ ) was varied  
15 from 75 to 375 m with increasing altitude. Ozone number concentration profiles were  
16 computed from the differential of the logarithm of the ratio of the signals by fitting a  
17 third-order polynomial to nine adjacent signals by the least-mean-squares method  
18 (Fujimoto and Uchino, 1994). The effective vertical resolution was about  $9 \cdot \Delta z \cdot 0.4 =$   
19  $3.6 \cdot \Delta z$ , which was estimated from the full-width half-maximum of the ozone profiles  
20 retrieved when an impulse function of ozone density was input (Beyerle and McDermid,  
21 1999). To calculate atmospheric molecular extinction, we used the atmospheric  
22 molecular extinction cross section (Bucholtz, 1995) and the atmospheric molecular  
23 density obtained from radiosonde data at the Fukuoka District Meteorological  
24 Observatory (33.58°N, 130.38°E). The ozone absorption cross sections were calculated  
25 by taking temperature dependence into account (Bass, 1984). The ozone volume mixing  
26 ratio was also calculated from the molecular density, including water vapor.

27 An example of DIAL measurements using four wavelengths, including 312 nm, is  
28 shown in Fig. 2. In this case, vertical profiles of the ozone number density and volume  
29 mixing ratio are plotted together with their statistical errors (precision) calculated from  
30 the lidar signal-to-noise ratios (Uchino and Tabata, 1991). A different wavelength pair  
31 was used for each of three altitude ranges to adapt to different ozone optical depths:  
32 276/288 nm for 1.0–3.0 km ( $\Delta z = 75$  m), 287/299 nm for 1.6–8.0 km ( $\Delta z = 150$  m) and  
33 8.0–18.6 km ( $\Delta z = 375$  m), and 299/312 nm for 17.4–20.8 km ( $\Delta z = 375$  m). The  
34 integration time was about 6 h to observe ozone vertical profiles up to 20 km (Fig. 2),  
35 but ozone vertical profiles up to 6 km were usually obtained within 30 min. From  
36 January through September 2012, we generally used an integration time of about 1–3 h

1 for biaxial and coaxial DIAL measurements, thus the resulting measurement errors  
2 were larger than those shown in Fig. 2. In this paper, we present the 2012 ozone data for  
3 altitudes lower than 6 km, measured by the DIAL system using three wavelengths (276,  
4 287, and 299 nm). In this DIAL data analysis, the systematic **uncertainty** (accuracy) due  
5 to particulate backscatter and extinction was not taken into account. However,  
6 systematic **uncertainty** is probably on the order of 10–15 % in the planetary boundary  
7 layer and smaller than that in the free troposphere (Nakazato et al., 2007), **although it**  
8 **can reach high values due to the presence of high aerosol loadings and the large aerosol**  
9 **concentration gradient at the top of the PBL (Papayannis et al., 1990).**

10 We compared our DIAL measurement with ozonesonde data (Thompson et al., 2011)  
11 (Fig. 3). The ozonesondes used were composed of an ECC ozone sensor (ENSCI-Z) and a  
12 GPS radiosonde (Meisei RS-06G). The precision and accuracy of the ozone sensor were  
13  $\pm 4$  % and  $\pm 5$  % at 1000 hPa and  $\pm 12$  % and  $\pm 12$  % at 200 hPa, respectively, and the  
14 vertical resolution of the sensor was 300 m  
15 ([http://www.dropletmeasurement.com/products/airborne/ECC\\_Ozonesonde](http://www.dropletmeasurement.com/products/airborne/ECC_Ozonesonde)). Two  
16 ozonesondes were launched by the Japan Weather Association under contract with  
17 NIES, and the measurements used in our comparison were made on 9 and 15 January  
18 2013. The ozonesonde and DIAL measurement times were from 12:31 to 13:53 LT and  
19 from 12:46 to 13:30 LT, respectively, on 9 January. On 15 January, the ozonesonde  
20 measurement time was from 12:31 to 14:04 LT under cloudy conditions, and we used  
21 DIAL data obtained from 14:00 to 17:04 LT under comparatively clear weather  
22 conditions for the comparison. The vertical resolution of the DIAL measurement was  
23 110 m in the lower altitude range and 830 m in the upper altitude range. Within their  
24 measurement errors, the ozonesonde and DIAL data were consistent below an altitude  
25 of 6 km (Fig. 3). **The average and one standard deviation of the difference between DIAL**  
26 **and ozonesonde data are  $14 \pm 10$  % below 2 km,  $6 \pm 4$  % for 2–7 km, and  $20 \pm 13$  % above 7**  
27 **km.**

### 30 **3 MRI-CCM2**

31  
32 The MRI-CCM2 model uses chemical and physical processes from the surface to the  
33 stratosphere to simulate the global distribution and evolution of ozone and other trace  
34 gases (Deushi and Shibata, 2011). The previous version (MRI-CCM1) was a  
35 stratospheric chemistry-climate model (Shibata et al., 2005). Version 2, however,  
36 incorporates an elaborated mechanism for HO<sub>x</sub>-NO<sub>x</sub>-CH<sub>4</sub>-CO photochemistry and

1 mechanisms for the degradation of non-methane hydrocarbons and heterogeneous  
2 tropospheric reactions of aerosols, so it can simulate tropospheric ozone chemistry as  
3 well as stratospheric chemistry. Deushi and Shibata (2011) showed that MRI-CCM2 can  
4 reproduce reasonably well the observed seasonal variations of the monthly means of  
5 ozone and carbon monoxide in the troposphere. This model is currently used to predict  
6 the distribution of photochemical oxidants near the surface in support of operational  
7 air-quality forecasts of the Japan Meteorological Agency (JMA). As first step toward  
8 better air quality prediction using the model, it is necessary to evaluate MRI-CCM2 by  
9 various observational data. It is important to compare ozone data predicted by the  
10 model with not only surface ozone data but also vertical ozone data.

11 The chemistry module of MRI-CCM2 considers 90 chemical species, 231 homogeneous  
12 gas-phase chemical reactions (172 chemical kinetic reactions and 59 photolysis  
13 reactions), and 16 heterogeneous reactions, and it incorporates grid-scale transport with  
14 a semi-Lagrangian scheme, sub-grid-scale convective transport and turbulent diffusion,  
15 dry and wet deposition, and emissions of trace gases from various sources. The  
16 chemistry module is coupled with an MRI atmospheric general circulation model  
17 (MRI-AGCM3; Yukimoto et al., 2011) via a simple coupler (Yoshimura and Yukimoto,  
18 2008). The chemistry module receives meteorological and radiation fields and surface  
19 conditions from MRI-AGCM3. The horizontal coordinate system of MRI-CCM2 is a  
20 Gaussian grid with a resolution of about 110 km. In the vertical, a hybrid p- $\sigma$  coordinate  
21 system is used, with 48 layers from the surface to the top of the atmosphere (0.01 hPa  $\approx$   
22 80 km). In the hybrid p- $\sigma$  coordinate system, the vertical coordinate is a  
23 terrain-following  $\sigma$ -coordinate ( $\sigma = p/p_s$ ) near the surface, and it gradually changes to a  
24 pressure coordinate (p-coordinate) near the top. The vertical resolution increases from  
25 about 100 to 600 m from the surface to 6 km. The time step of the transport (chemistry)  
26 scheme is 30 (15) minutes.

27 In this study, the horizontal wind field in AGCM3 was forced toward the observed field  
28 by using a nudging assimilation with an 18 h e-folding time. JMA operational analysis  
29 data were used as the observed wind field for the nudging assimilation. In the  
30 chemistry module, trace gas emissions from the burning of fossil fuels by industrial  
31 activities and aircraft (anthropogenic sources), from biomass burning (anthropogenic  
32 and natural sources), and from vegetation, soils, and the ocean (natural sources) were  
33 prescribed. Global anthropogenic emission data, except those from East Asia, were  
34 obtained from the inventory in the Emission Database for Global Atmospheric Research  
35 (EDGAR) v2.0 (Olivier et al., 1996) modified by the seasonal adjustments of Müller  
36 (1992). For East Asia, the prescribed data were obtained from an inventory of Asian

1 anthropogenic emissions, the Regional Emission inventory in ASia (REAS), version 1.1  
2 (Ohara et al., 2007). Biogenic and oceanic emissions were taken from Horowitz et al.  
3 (2003) and references therein. Emission of NO<sub>x</sub> from lightning was diagnosed at 6 h  
4 intervals in the chemistry module by using the meteorological fields from AGCM3 (for  
5 details, see Deushi and Shibata, 2011). Emission of trace gases from biomass burning,  
6 which depends on the height above ground, is based on the Description of EDGAR  
7 32FT2000(v8)  
8 ([http://www.rivm.nl/edgar/Images/Description\\_of\\_EDGAR\\_32FT2000\(v8\)\\_tcm32-22222.](http://www.rivm.nl/edgar/Images/Description_of_EDGAR_32FT2000(v8)_tcm32-22222.pdf)  
9 pdf). Present-day concentrations of N<sub>2</sub>O, CH<sub>4</sub>, chlorofluorocarbons, and halons were  
10 prescribed at the surface. In this paper we used the data output by the model every hour  
11 for the comparison with the DIAL-observed data in this study.

#### 12 13 14 **4 DIAL observational results and comparison with MRI-CCM2 output**

15  
16 Hourly grid-point ozone data predicted by MRI-CCM2 were spatially interpolated for  
17 the Saga area, averaged over the DIAL measurement time (about 1–7 hrs), and then  
18 compared to our DIAL ozone data.

##### 19 20 **4.1 Vertical profiles**

21  
22 At first the vertical profiles of lower tropospheric ozone in the altitude range of 1–6 km  
23 measured by DIAL between January and May 2012 are compared with MRI-CCM2  
24 predictions (Fig. 4). The DIAL-measured ozone volume mixing ratios on 30 January,  
25 being of about 40–50 ppbv were successfully predicted by MRI-CCM2, except in the 4–5  
26 km altitude range. High ozone values were measured at around 2 km altitude in the  
27 daytime on 23 April, 5 May, and 11 May. A backward trajectory analysis suggested that  
28 the air masses linked with these high ozone volume mixing ratios at 2 km were  
29 transported to Saga across the Yellow Sea (23 April and 5 May) or over the Korean  
30 Peninsula (11 May) from polluted areas in East China (Parrish and Zhu, 2009) within a  
31 few days. MRI-CCM2 predicted well these high ozone densities on 23 April, but not  
32 those on 5 May or 11 May. This is possibly in part because emissions were assumed in  
33 the model to be constant (climatological data were used).

34 Figure 5 shows ozone profiles in the 1–6 km altitude range for July and September  
35 2012. MRI-CCM2 was unable to predict the high ozone values of more than 70 ppbv  
36 above 2.3 km that were measured by DIAL on 7 July. On 19 July, the measured ozone

1 volume mixing ratios were 10–30 ppbv below about 4 km, whereas MRI-CCM2  
2 predicted ratios of 30–40 ppbv below 4 km. On 28 July, however, MRI-CCM2 predicted  
3 well the ozone volume mixing ratios measured by DIAL of about 30–40 ppbv below 4 km.  
4 On 26 September, MRI-CCM2 predicted very well the ozone volume mixing ratios  
5 measured by DIAL of about 35–70 ppbv from 500 m to 6 km. According to the backward  
6 trajectory analysis, the air masses below 4 km with low ozone volume mixing ratios of  
7 about 20–40 ppbv on 19 and 28 July came from the Pacific Ocean south of Saga. The  
8 ozone volume mixing ratios predicted by MRI-CCM2 for 2–6 km on 7 July were lower,  
9 and those for 1–4 km on 19 July were higher, compared with the DIAL measurements.

10 Figure 6 shows horizontal maps of ozone volume mixing ratio and horizontal wind  
11 predicted by MRI-CCM2 for 500 hPa (about 5.5 km altitude), 700 hPa (3 km), 800 hPa (2  
12 km), and 850 hPa (1.5 km) pressure levels at 06 UTC on 7 July 2012. According to the  
13 weather chart on the same day provided by JMA  
14 (<http://www.data.jma.go.jp/fcd/yoho/hibiten/index.html>), the Meiyu-Baiu-front extended  
15 from west to east through the center of a low-pressure system over Japan. In this  
16 prediction, the synoptic-scale pattern of horizontal-wind field is reproduced reasonably.  
17 A large north-south gradient of ozone volume mixing ratios is located near the  
18 stationary front in the lower free-troposphere. The ozone concentration is low over the  
19 south part of the front because of the chemical destruction in the summertime marine  
20 air mass, whereas high ozone level area is present over the north of the front. During  
21 the DIAL observing period the large gradient of ozone concentration was located near  
22 the Saga site in the lower free-troposphere (Fig.6). This suggests that one of the possible  
23 reasons for the significant discrepancy between the DIAL ozone profile and the  
24 predicted one (Fig. 5) is that the meso-scale front structure and its position are not fully  
25 captured by the model due to its coarse spatial resolution. In addition, it is plausible  
26 that model transport with the coarse grid doesn't reproduce well fine-scale structures of  
27 air (trace gases) filaments.

## 28 29 **4.2 Lower tropospheric ozone column**

30  
31 Figure 7 shows time variations of the lower tropospheric ozone column amounts within  
32 the 1–6 km and 1–2 km altitude ranges over Saga in 2012 as measured by DIAL and  
33 predicted by MRI-CCM2. Because of restricting weather conditions, DIAL  
34 measurements were obtained only twice in May and twice in June, but at least three  
35 measurements were obtained in each of the other months. In 2012, the ozone column  
36 amounts showed an approximately seasonal variation except for a dip from early July

1 through mid-September. Column amounts within 1–6 km were almost constant from  
2 January to early March, and then increased until late June. The maximum value in the  
3 1–6 km range was  $7.82 \times 10^{21}$  molecules  $\text{m}^{-2}$ , corresponding to 29.1 DU (1 DU =  $2.688 \times$   
4  $10^{20}$  molecules  $\text{m}^{-2}$ ), on 22 June 2012. Thereafter, ozone column amounts within the 1–6  
5 km range decreased to early August, but with large variations. The minimum value  
6 within the 1–6 km range of  $2.28 \times 10^{21}$  molecules  $\text{m}^{-2}$  (8.5 DU) was observed on 15  
7 August 2012. These variations are due to possibly exchange events between the  
8 ozone-rich continental and the ozone-poor maritime air masses. Subsequently, ozone  
9 column amounts increased again to mid-September, and then decreased slowly,  
10 becoming almost constant by December, when the ozone column amount within the 1–6  
11 km range was  $4.65 \times 10^{21}$  molecules  $\text{m}^{-2}$  (17.3 DU). The results predicted by MRI-CCM2  
12 were mainly consistent with our DIAL observational results.

13 The temporal variation of the ozone column values within the 1–2 km range in 2012  
14 was similar to that in the 1–6 km range. The mean value was about  $1.03 \times 10^{21}$   
15 molecules  $\text{m}^{-2}$  (3.8 DU) from 20 January to 11 February. Then, the ozone column  
16 amount increased to a maximum value of  $2.02 \times 10^{21}$  molecules  $\text{m}^{-2}$  (7.5 DU) on 5 May,  
17 followed by a decreased value down to  $0.32 \times 10^{21}$  molecules  $\text{m}^{-2}$  (1.2 DU) on 19 July.  
18 Moreover the mean ozone column amount within the 1–2 km range was about  $0.55 \times$   
19  $10^{21}$  molecules  $\text{m}^{-2}$  (2.0 DU) from 28 July to 18 August. Subsequently, the column ozone  
20 value increased to more than  $1.0 \times 10^{21}$  molecules  $\text{m}^{-2}$  (3.7 DU) by 19 December.  
21 MRI-CCM2 predicted similar variations of the ozone column amounts within the 1–2  
22 km range, but the predicted values were lower than the DIAL measurements on 5 and  
23 11 May and 22 June.

## 24 25 26 **5 Concluding remarks**

27  
28 With our improved DIAL system, 44 ozone profiles were observed in the 1–6 km altitude  
29 range over Saga in 2012. High ozone layers were observed at around 2 km altitude  
30 during April and May. Ozone column amounts within the 1–6 km altitude range were  
31 almost constant (19.1 DU) from January to March, and increased to 26.7 DU from late  
32 April to July. From mid-July through August, ozone column amounts showed large  
33 variations (8.5–22.0 DU), attributed to exchanges between continental and maritime air  
34 masses. Ozone column amounts within the 1–6 km range increased again to  
35 mid-September, then decreased slowly to 17.3 DU and became almost constant through  
36 December.

1 MRI-CCM2 successfully predicted these ozone variations with the following  
2 exceptions. MRI-CCM2 could not predict the high ozone volume mixing ratios measured  
3 at around 2 km altitude on 5 May and 11 May, possibly in part because emissions  
4 (especially from open biomass burning) were assumed in the model to be constant  
5 (climatological data were used). Ozone volume mixing ratios predicted by MRI-CCM2  
6 were low in the 2–6 km range on 7 July and high in the 1–4 km range on 19 July  
7 compared with those measured by DIAL.

8 A major benefit of ozone DIAL is that it can measure continuously vertical ozone  
9 profiles with high vertical and temporal resolution. The process of stratospheric ozone  
10 intrusion into the troposphere was clearly observed on 20-21 June 2001 by continuous  
11 DIAL measurement at Garmisch-partenkichen, Germany and the excellent data set  
12 was used for model intercomparisons and validation (Roelofs et al., 2003; Zanis et al.,  
13 2003; Stohl et al., 2003). On the other hand, the ability of a regional air quality model  
14 was evaluated to reproduce summertime ozone pollution over the Kanto region in Japan  
15 using quasi-continuous ozone DIAL measurement data (Niwano et al, 2007). We plan to  
16 study the process that air mass of high ozone concentration in the free troposphere is  
17 mixed into the planetary boundary layer by continuous DIAL measurement. Further,  
18 we plan to utilize ozone DIAL data for validation of a new version of an MRI oxidant  
19 prediction system over an extended period of time. In the prediction system, a regional  
20 chemistry-transport model, known as MRI-PM/c (Kajino et al., 2012), with higher  
21 spatial resolution (20 km and/or 5 km) is nested in MRI-CCM2. The prediction system  
22 also adopts an up-to-date inventory and higher temporal resolution of biomass burning  
23 emissions. The regional model can reproduce meso-scale weather phenomena and  
24 advection of air mass. However, if boundary data for the regional model produced by the  
25 global model doesn't include adequate information on fine-scale structures in trace gas  
26 distributions, the performance of the prediction system will be degraded. Therefore, in  
27 order to improve total performance of the prediction system, it is necessary to validate  
28 not only the regional model but also the global model with observation data such as  
29 ozone DIAL data and surface ozone monitoring data extensively, which enable us to  
30 estimate error coming from outside of the boundary.

31  
32 *Acknowledgements.* We used radiosonde data measured by the Japan Meteorological  
33 Agency, and the Meteorological Data Explorer (METEX), developed by Jiye Zeng at the  
34 Center for Global Environmental Research (CGER) of NIES to calculate isentropic  
35 backward trajectories. This work was partly supported by JSPS KAKENHI Grant  
36 Number 23310018.

## 1 **References**

- 2 Ancellet, G., Papayannis, A., Pelon, J., and Mégie, G.: DIAL tropospheric ozone  
3 measurement using a Nd:YAG laser and the Raman shifting technique, *J. Atmos.*  
4 *Ocean. Technol.*, 6, 832-839, 1989.
- 5 Apituley, A., Hoexum M., Potma, C., and Wilson, K.: Tropospheric ozone DIAL for air  
6 quality and climate monitoring, and validation studies, *Proceedings of the 25<sup>th</sup>*  
7 *International Laser Radar conference, St.-Petersburg, 5-9 July 2010*, p862-865.
- 8 Bass, A. M.: The ultraviolet absorption cross-section of ozone, *Fin. Rep. NASA, Cont. No.*  
9 *S-40127B*, 1984.
- 10 Beyerle, G. and McDermid, I. S.: Altitude range resolution of differential absorption  
11 lidar ozone profiles, *Appl. Opt.*, 38, 924-927, 1999.
- 12 Browell, E. V., Carter, A. F., Shipley, S. T., Allen, R. J., Butler, C. F., Mayo, M. N., Siviter,  
13 Jr., J. H., and Hall, W. M.: NASA multipurpose airborne DIAL system and  
14 measurements of ozone and aerosol profiles, *Appl. Opt.*, 22, 522-534, 1983.
- 15 Bucholtz, A.: Rayleigh-scattering calculations for the terrestrial atmosphere, *Appl. Opt.*,  
16 34, 2765-2773, 1995.
- 17 Deushi, M. and Shibata, K.: Development of a Meteorological Research Institute  
18 Chemistry-Climate Model version 2 for the study of tropospheric and stratospheric  
19 chemistry, *Pap. Meteorol. Geophys.*, 62, 1-46, doi:10.2467/mripapers.62.1, 2011.
- 20 Eisele, H., Scheel, H. E., Sladkovic, R., and Trickl, T.: High-resolution lidar  
21 measurements of stratosphere-troposphere exchange, *J. Atmos. Sci.*, 319-330, 1999.
- 22 Fujimoto, T. and Uchino, O.: Estimation of the error caused by smoothing on DIAL  
23 measurements of stratospheric ozone, *J. Meteor. Soc. Jpn.*, 72, 605-611, 1994.
- 24 Gibson, A. J. and Thomas, L.: Ultraviolet laser sounding of the troposphere and lower  
25 stratosphere, *Nature*, 256, 561-563, 1975.
- 26 Godin-Beekmann, S., Porteneuve, J., and Garnier, A.: Systematic DIAL lidar  
27 monitoring of the stratospheric ozone vertical distribution at Observatoire de  
28 Haute-Provence (43.92°N, 5.71°E), *J. Environ. Monitor.*, 5, 57-67, 2003.
- 29 Horowitz, L. W., Walters, S. M., Mauzerall, D. L., Emmons, L. K., Rasch, P. J., Granier,  
30 C., Tie, X., Lamarque, J.-F., Schultz, M. G., Tyndall, G. S., Orlando, J. J., and  
31 Brasseur, G. P.: A global simulation of tropospheric ozone and related tracers:  
32 description and evaluation of MOZART, version 2. *J. Geophys. Res.*, 108, D24, 4784,  
33 doi:10.1029/2002JD002853, 2003.
- 34 Intergovernmental Panel on Climate Change (IPCC), *Climate change 2007: The*  
35 *Physical Science Basis: Contribution of Working Group I to the Fourth Assessment*  
36 *Report of the Intergovernmental Panel on Climate Change*, edited by Solomon, S.,

1     Qin, S., Manning, M., Chen, Z., Marquis, M., Averyt, K. B., Tignor, M., and Miller, H.  
2     L., Cambridge University Press, Cambridge, UK and New York, NY, USA, 996pp.  
3     2007.

4     Kajino, M., Deushi, M., Maki, T., Oshima, N., Inomata, Y., Sato, K., Ohizumi, T., and  
5     Ueda, H.: Modeling wet deposition and concentration of inorganics over Northeast  
6     Asia with MRI-PM/c, *Geosci. Model Dev.*, 5, 1363-1375, doi:10.5194/gmd-5-1363-2012,  
7     2012.

8     Kempfer, U., Carnuth, W., Lotz, R., and Trickl, T.: A wide-range ultraviolet lidar system  
9     for tropospheric ozone measurements: development and application, *Rev. Sci.*  
10    *Instrum.*, 65, 3145-3164, 1994.

11    Kuang, S., Newchurch, M. J., Burris, J., and Liu, X.: Ground-based lidar for  
12    atmospheric boundary layer ozone measurements, *Appl. Opt.*, 52, 3557-3566, 2013.

13    McDermid, I. S., Beyerle, G., Haner, D. A., and Leblanc, T.: Redesign and improved  
14    performance of the tropospheric ozone lidar at the Jet Propulsion Laboratory Table  
15    Mountain Facility, *Appl. Opt.*, 41, 7550-7555, 2002.

16    Müller, J. F.: Geographical distribution and seasonal variation of surface emissions and  
17    deposition velocities of atmospheric trace gases. *J. Geophys. Res.*, 97, 3787-3804,  
18    1992.

19    Nakazato, M., Nagai, T., Sakai, T., and Hirose, Y.: Tropospheric ozone  
20    differential-absorption lidar using stimulated Raman scattering in carbon dioxide,  
21    *App. Opt.*, 46, 2269-2279, 2007.

22    Niwano, M., Takigawa, M., Takahashi, M., Akimoto, H., Nakazato, M., Nagai, T., Sakai,  
23    T., and Mano, Y.: Evaluation of vertical ozone profiles simulated by WRF/Chem using  
24    lidar-observed data, *SOLA*, 3, 133-136, doi:10.2151/sola.2007-034, 2007.

25    Ohara, T., Akimoto, H., Kurokawa, J., Horii, N., Yamaji, K., Yan, X., and Hayasaka, T.:  
26    An Asian emission inventory of anthropogenic emission sources for the period of  
27    1980-2020, *Atmos. Chem. Phys.*, 7, 4419-4444, 2007.

28    Ohyama, H., Kawakami, S., Shiomi, K., and Miyagawa, K.: Retrievals of total and  
29    tropospheric ozone from GOSAT thermal infrared spectral radiances, *IEEE Trans.*  
30    *Geosci. Remote Sens.*, 50, 1770–1784, doi:10.1109/TGRS.2011.2170178, 2012.

31    Olivier, J. G. J., Bouwman, A. F., van der Maas, C. W. M., Berdowski, J. J. M., Veldt, C.,  
32    Bloos, J. P. J., Visschedijk, A. J. H., Zandveld, P. Y. J., and Haverlag, J. L.: Description  
33    of EDGAR version 2.0: a set of global emission inventories of greenhouse gases and  
34    ozone-depleting substances for all anthropogenic and most natural sources on a per  
35    country basis and on 1° ×1° grid. RIVM Rep. 771060 002/TNO-MEP Rep. R96/119,  
36    National Institute of Public Health and Environment, Bilthoven, Netherlands, 1996.

1 Papayannis, A., Ancellet, G., Pelon, J., and Mégie, G.: Multiwavelength lidar for ozone  
2 measurements in the troposphere and the lower stratosphere, *Appl. Opt.*, 29, 467-476,  
3 1990.

4 Papayannis, A., Balis, D., Zanis, P., Galani, E., Wernli, H., Zerefos, C., Stohl, A.,  
5 Eckhardt, S., and Amiridis, V.: Sampling of an STT event over the Eastern  
6 Mediterranean region by lidar and electrochemical sonde, *Annales Geophys.*, 23,  
7 2039-2050, 2005.

8 Parrish, D. D., and Zhu, T.: Clean air for megacities, *Science*, 326, 674-675,  
9 doi:10.1126/science.1176064.

10 Parrish, D. D., Law, K. S., Staehelin, J., Derwent, R., Cooper, O. R., Tanimoto, H.,  
11 Volz-Thomas, A., Gilge, S., Scheel, H. -E., Steinbacher, M., and Chan, E.: Long-term  
12 changes in lower tropospheric baseline ozone concentrations at northern  
13 mid-latitudes, *Atmos. Chem. Phys.*, 12, 11485-11504, doi:10.5194/acp-12-11485-2012,  
14 2012.

15 Pelon, J., and Mégie, G.: Ozone monitoring in the troposphere and lower stratosphere:  
16 evaluation and operation of a ground-based lidar station, *J. Geophys. Res.*, 87,  
17 4947-4955, 1982.

18 Proffitt, M. H. and Langford, A. O.: Ground-based differential absorption lidar system  
19 for day or night measurements of ozone throughout the free troposphere, *Appl. Opt.*,  
20 36, 2568-2585, 1997.

21 Roelofs, G. J., Kentarchos, A. S., Trickl, T., Stohl, A., Collins, W. J., Crowther, R. A.,  
22 Hauglustaine, D., Klonecki, A., Law, K. S., Lawrence, M. G., von Kuhlmann, R., and  
23 van Weele, M.: Intercomparison of tropospheric ozone models: ozone transport in a  
24 complex tropopause folding event, *J. Geophys. Res.*, 108, D12, 8529,  
25 doi:10.1029/2003JD003462, 2003.

26 Seabrook, J. A., Whiteway, J., Staebler, R. M., Bottenheim, J. W., Komguem, L., Gray, L.  
27 H., Barber, D., and Asplin, M.: LIDAR measurements of Arctic boundary layer ozone  
28 depletion events over the frozen Arctic Ocean, *J. Geophys. Res.*, 116, D00S02,  
29 doi:10.1029/2011JD016335, 2011.

30 Shibata, K., M. Deushi, T. T. Sekiyama, and H. Yoshimura: Development of an MRI  
31 chemical transport model for the study of stratospheric chemistry. *Pap. Geophys.*  
32 *Meteorol.*, 55, 75-119, 2005.

33 Stohl, A., Bonasoni, P., Cristofanelli, P., Collins, W., Feichter, J., Frank, A., Forster, C.,  
34 Gerasopoulos, E., Gäggeler, H., James, P., Kentarchos, T., Kromp-Kolb, H., Kruöger,  
35 B., Land, C., Meloan, J., Papayannis, A., Priller, A., Seibert, P., Sprenger, M., Roelofs,  
36 G. J., Scheel, H. E., Schnabel, C., Siegmund, P., Tobler, L., Trickl, T., Wernli, H.,

1     Wirth, V., Zanis, P., and Zerefos, P.: Stratosphere-troposphere exchange: a review,  
2     and what we have learned from STACCATO, *J. Geophys. Res.*, 108, D12, 8516,  
3     doi:10.1029/2002JD002490, 2003.

4     Sunesson, J. A., Apituley, A., and Swart, D. P. J.: Differential absorption lidar system for  
5     routine monitoring of tropospheric ozone, *Appl. Opt.*, 33, 7045-7058, 1994.

6     Thompson, A. M., Oltmans, S. J., Tarasick, D. W., Von der Gathen, P., Smit, H. G. J., and  
7     Witte, J. C.: Strategic ozone sounding networks: review of design and  
8     accomplishments, *Atmos. Environ.* 45, 2145-2163, 2011.

9     Uchino, O. and Tabata, I.: Mobile lidar for simultaneous measurements of ozone,  
10    aerosols, and temperature in the stratosphere, *Appl. Opt.*, 30, 2005-2012, 1991.

11    Uchino, O., Tokunaga, M., Maeda, M., and Miyazoe, Y.: Differential-absorption-lidar  
12    measurement of tropospheric ozone with excimer-Raman hybrid laser, *Opt. Lett.*, 8,  
13    347-349, 1983.

14    Uchino, O., Sakai, T., Nagai, T., Nakazato, M., Morino, I., Yokota, T., Matsunaga, T.,  
15    Sugimoto, N., Arai, K., and Okumura, H.: Development of a mobile lidar for GOSAT  
16    product validation, *J. Remote Sens. Soc. Jpn.*, 31, 435-445, 2011 (in Japanese)

17    Wang, Y., Konopka, P., Liu, Y., Che, H., Muller, R., Müller, R., Plöger, F., Riese, M., Cai,  
18    Z., and Lü, D.: Tropospheric ozone trend over Beijing from 2002-2010: ozonesonde  
19    measurements and modeling analysis, *Atmos. Chem. Phys.*, 12, 8389-8399,  
20    doi:10.5194/acp-12-8389-2012, 2012.

21    Yoshimura, H., and Yukimoto S.: Development of a Simple Coupler (Scup) for Earth  
22    System Modeling. *Pap. Meteor. Geophys.*, 59, 19-29, 2008.

23    Yukimoto, S., Yoshimura, H., Hosaka, M., Sakami, T., Tsujino, H., Hirabara, M., Tanaka,  
24    T. Y., Deushi M., Obata, A., Nakano, H., Adachi, Y., Shindo, E., Yabu, S., Ose, T., and  
25    Kitoh, A.: Meteorological Research Institute Earth System Model Version 1  
26    (MRI-ESM1)—Model Description—, *Tech. Rep. of MRI*, 64, 83 pp, 2011.

27    Zhang, Q., Streets, D. G., He, K., Wang, Y., Richter, A., Burrows, J. P., Uno, I., Jang, C.  
28    J., Chen, D., Yao, Z., and Lei, Y.: NO<sub>x</sub> emission trends for China, 1995-2004: The view  
29    from the ground and the view from space, *J. Geophys. Res.*, 112, D22306,  
30    doi:10.1029/2007JD008684, 2007.

31    Zanis, P., Trickl, T., Stohl, A., Wernli, H., Cooper, O., Zerefos, C., Gaeggeler, H., Schnabel,  
32    C., Tobler, L., Kubik, P. K., Priller, A., Scheel, H. E., Kanter, H. J., Cristofanelli, P.,  
33    Forster, C., James, P., Gerasopoulos, E., Delcloo, A., Papayannis, A., and Claude, H.:  
34    Forecast, observation and modeling of a deep stratospheric intrusion event over  
35    Europe, *Atmos. Chem. Phys.*, 3, 763-777, 2003.

36

**Table 1.** Characteristics of tropospheric ozone DIAL system

|                       |                             |         |         |                             |         |  |
|-----------------------|-----------------------------|---------|---------|-----------------------------|---------|--|
| Transmitter           |                             |         |         |                             |         |  |
| Pump laser            | Nd:YAG                      |         |         |                             |         |  |
| Wavelength            | 266 nm                      |         |         |                             |         |  |
| Pulse energy          | 107 mJ                      |         |         |                             |         |  |
| Pulse repetition rate | 10 Hz                       |         |         |                             |         |  |
| Pulse width           | 8 ns                        |         |         |                             |         |  |
| Raman active gas      | CO <sub>2</sub>             |         |         |                             |         |  |
| Stokes lines          | 276 nm                      | 287 nm  | 299 nm  | 312 nm                      |         |  |
| Pulse energy          | 7.5 mJ                      | 9.1 mJ  | 8.4 mJ  | No. meas.                   |         |  |
| Beam divergence       | 0.1 mrad                    |         |         |                             |         |  |
| Receiver              |                             |         |         |                             |         |  |
| Telescope type        | Newtonian                   |         |         | Prime focus (fiber coupled) |         |  |
| Telescope diameter    | 49 cm                       |         |         | 10 cm                       |         |  |
| Focal length          | 1750 mm                     |         |         | 320 mm                      |         |  |
| Field of view         | 1 mrad                      |         |         | 3 mrad                      |         |  |
| Wavelength            | 287 nm                      | 299 nm  | 312 nm  | 276 nm                      | 287 nm  |  |
| Bandwidth             | 1.02 nm                     | 1.15 nm | 0.82 nm | 1.07 nm                     | 1.05 nm |  |
| Transmission          | 0.18                        | 0.32    | 0.36    | 0.17                        | 0.21    |  |
| Detector              | PMT (Hamamatsu R3235-01)    |         |         |                             |         |  |
| Signal processing     | 12bit A/D + Photon counting |         |         |                             |         |  |
| Time resolution       | 1 min                       |         |         |                             |         |  |
| Altitude resolution   | 7.5 m                       |         |         |                             |         |  |

1 **Figure captions**

2  
3 **Fig. 1.** Block diagram of tropospheric ozone DIAL system.

4 **Fig. 2.** Vertical profiles of ozone number density (left panel) and ozone volume mixing  
5 ratio (right panel) over Saga observed by DIAL on 20 October 2012. The error bars  
6 show the statistical errors calculated from the lidar signal to noise ratios.

7 **Fig. 3.** Comparison of ozone DIAL (black) and ECC ozonesonde (orange) measurements  
8 on 9 (left panel) and 15 January (right panel) in 2013. The error bars of ozone DIAL  
9 data show the statistical errors calculated from the lidar signal to noise ratios.

10 **Fig. 4.** Vertical profiles of ozone volume mixing ratios over Saga measured by DIAL  
11 (black lines) and predicted by MRI-CCM2 (orange lines) on 30 January, 23 April, 5  
12 and 11 May in 2012. The error bars shows the statistical errors calculated from the  
13 signal to noise ratios for the lidar and the standard deviation for the period predicted  
14 by MRI-CCM2.

15 **Fig. 5.** Same as Fig. 4 but for 7, 19, and 28 July, and 26 September in 2012.

16 **Fig. 6.** Horizontal maps of ozone volume mixing ratio in ppbv and horizontal wind in m/s  
17 predicted by MRI-CCM2 for 500, 700, 800, 850 hPa pressure levels at 06 h UTC on 7  
18 July 2012.

19 **Fig. 7.** Ozone columns for 1–6 km and 1–2 km altitude ranges over Saga in 2012  
20 measured by DIAL and predicted by MRI-CCM2.

21  
22

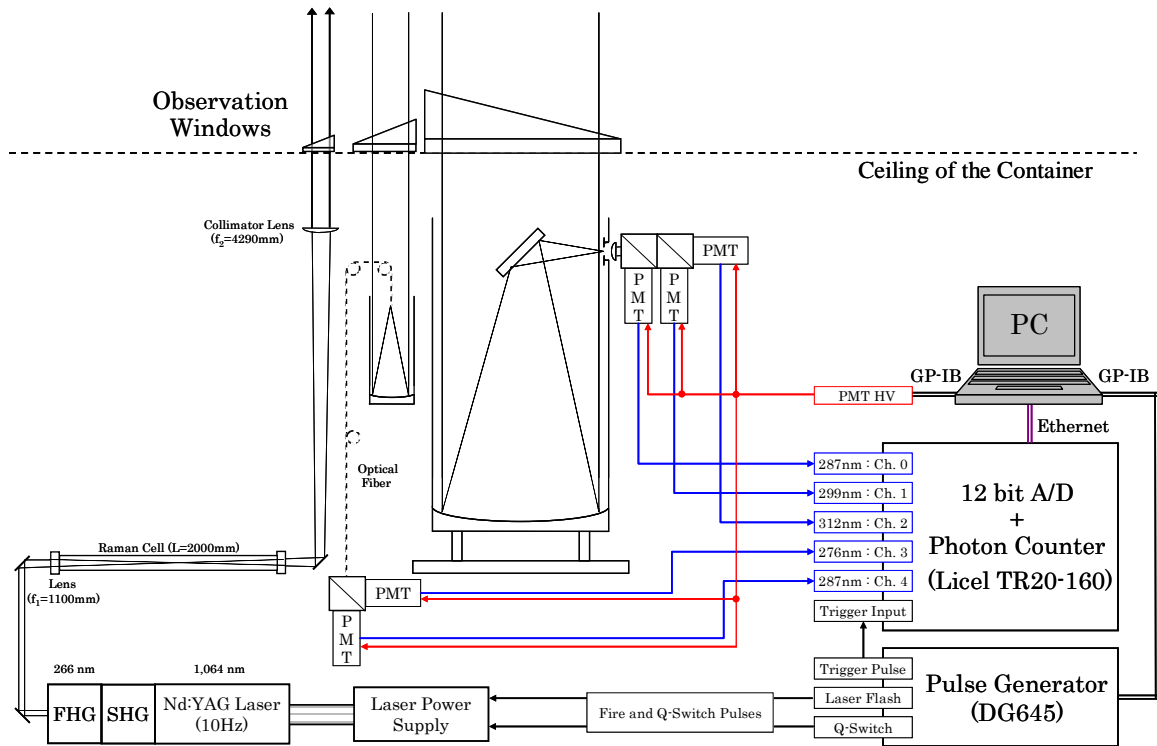


Fig. 1.

1  
2  
3  
4  
5  
6  
7  
8  
9  
10  
11  
12  
13  
14  
15  
16  
17  
18  
19  
20  
21

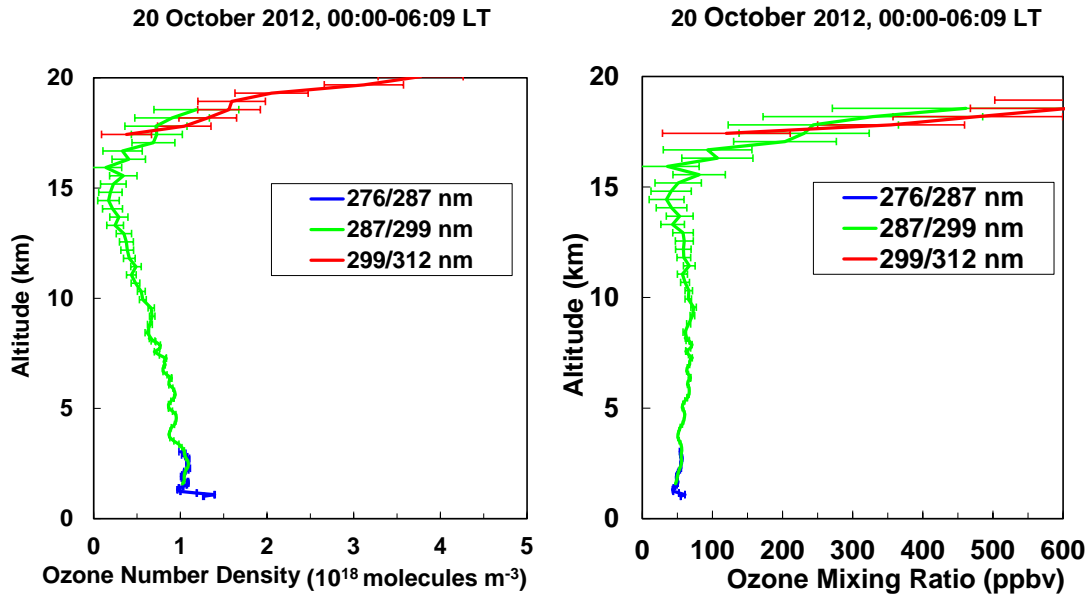


Fig.2

- 1
- 2
- 3
- 4
- 5
- 6
- 7
- 8
- 9
- 10
- 11
- 12
- 13
- 14
- 15
- 16
- 17
- 18
- 19
- 20
- 21
- 22
- 23
- 24

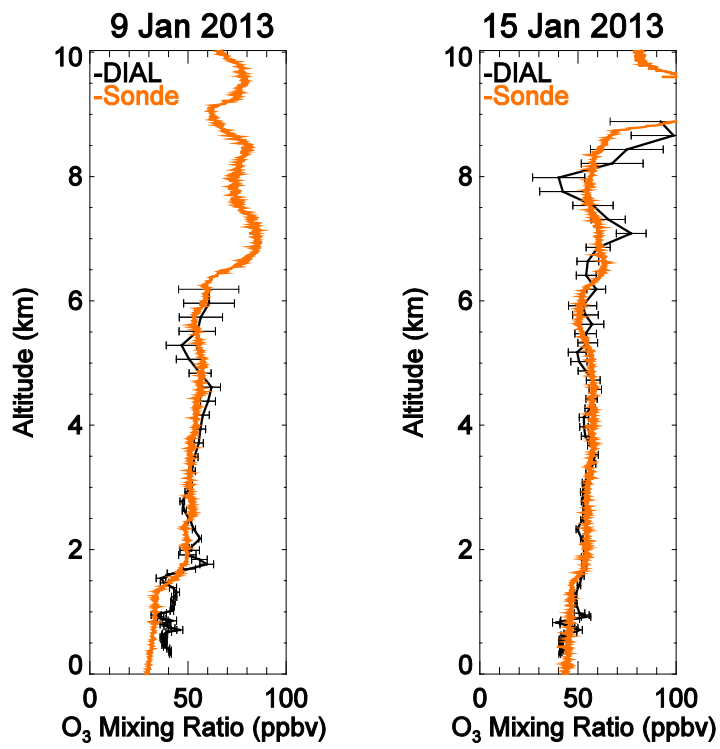


Fig. 3.

1  
2  
3  
4  
5  
6  
7  
8  
9  
10  
11  
12  
13  
14  
15  
16  
17  
18  
19  
20  
21

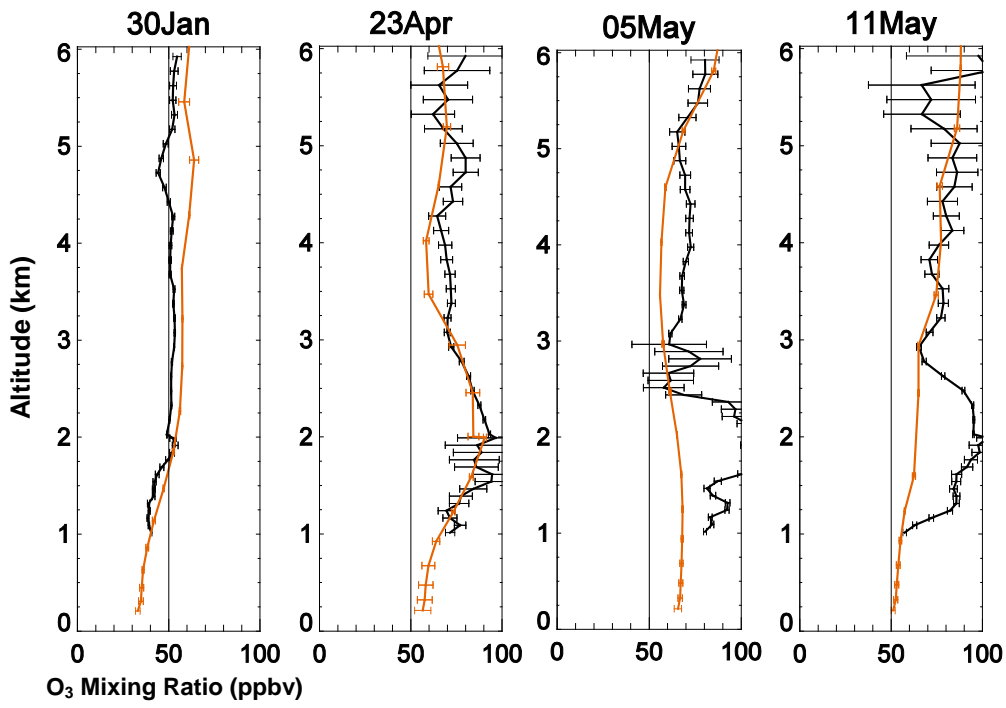


Fig. 4.

1  
2  
3  
4  
5  
6  
7  
8  
9  
10  
11  
12  
13  
14  
15  
16  
17  
18  
19  
20  
21  
22  
23  
24

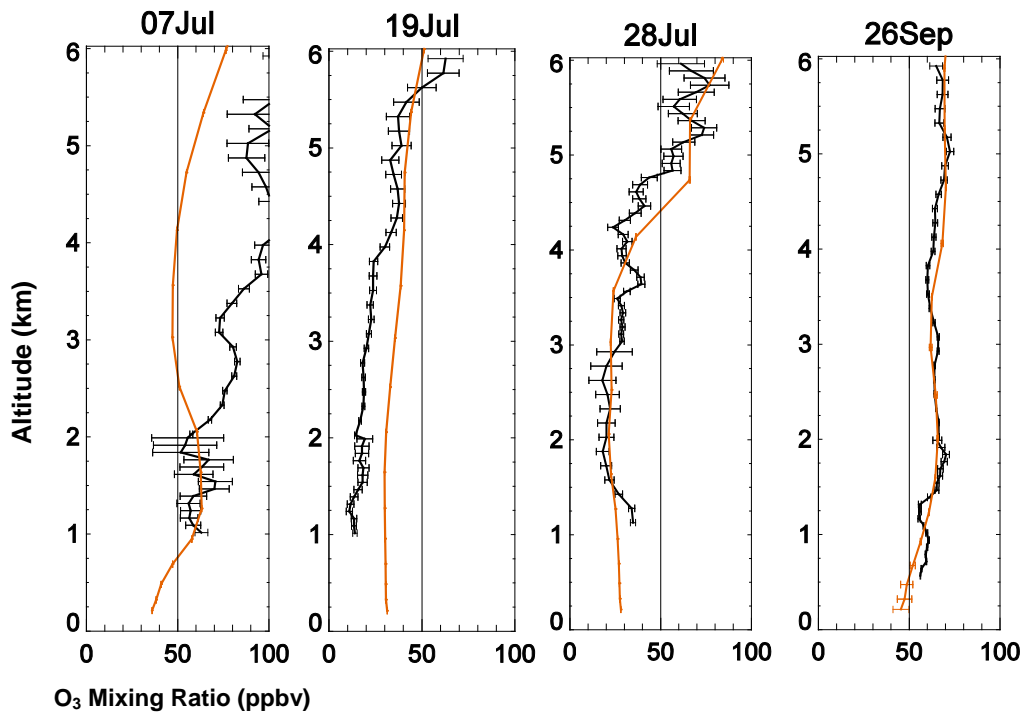
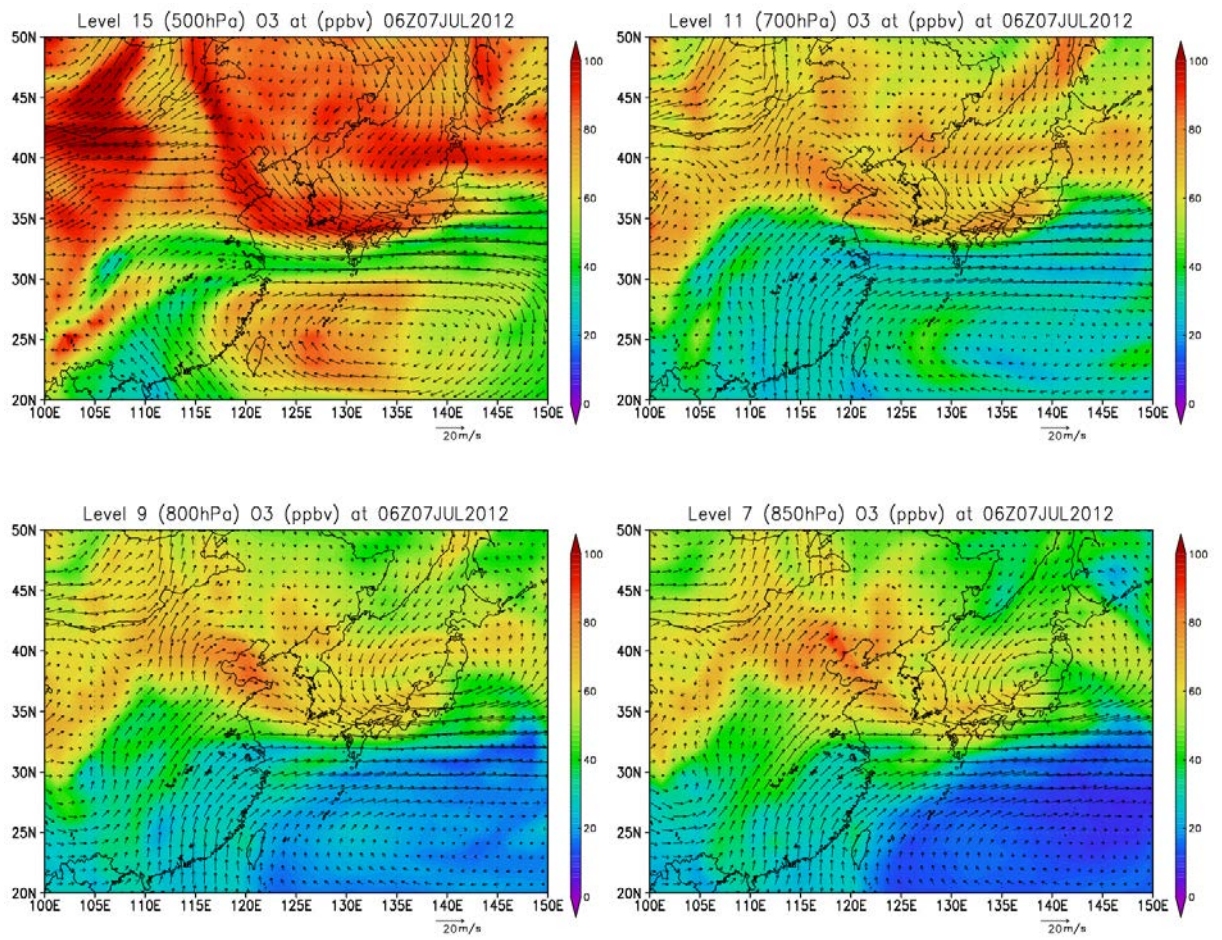


Fig. 5.

1  
2  
3  
4  
5  
6  
7  
8  
9  
10  
11  
12  
13  
14  
15  
16  
17  
18  
19  
20  
21  
22  
23

1



2

3

4

Fig. 6.

5

6

7

8

9

10

11

12

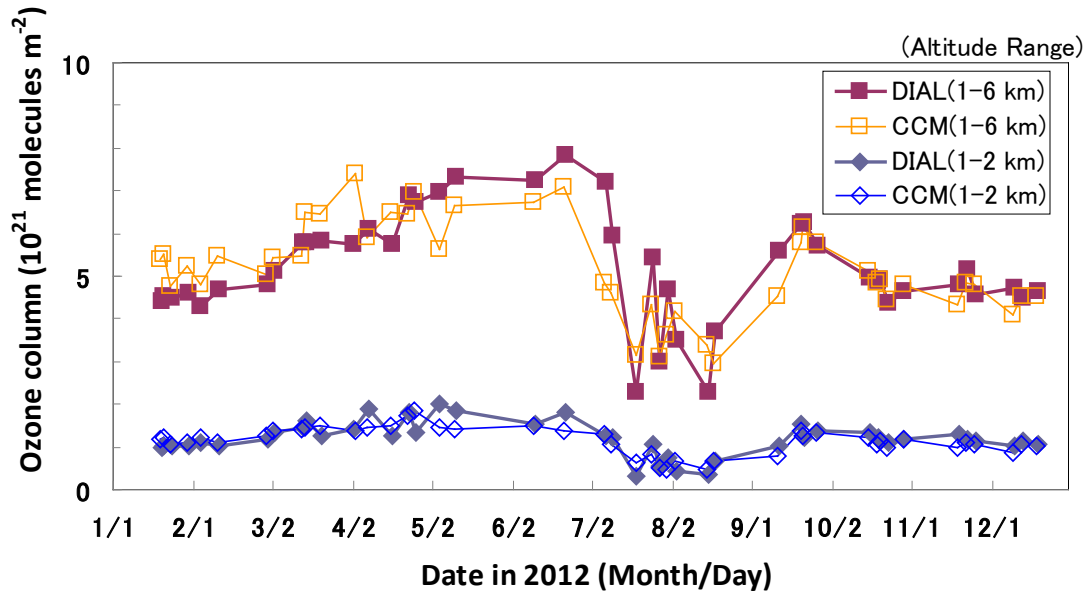
13

14

15

16

1



2

3

4

Fig. 7.